Modeling of Mobile Communication Systems by Electromagnetic Theory in the Direct and Single Reflected Propagation Scenario

Guo Sheng[1], Shuping Dang[2(✉)], Nadim Hossain[3], and Xu Zhang[4]

[1] Zhejiang Post and Telecommunication College,
Shaoxing 312016, People's Republic of China
sg@zptc.cn
[2] Department of Engineering Science, University of Oxford, Oxford OX1 3PJ, UK
shuping.dang@eng.ox.ac.uk
[3] School of Electrical and Electronic Engineering,
The University of Manchester, Manchester M13 9PL, UK
nadim5700@gmail.com
[4] Department of Mechanical Engineering and Materials Science,
Duke University, Durham, NC 27708-0287, USA
xz70@duke.edu

Abstract. In this paper, we employ electromagnetic theory to analyze the phenomenon of signal propagation and thereby model mobile communication systems. Using electromagnetic theory is different from conventional modeling techniques applied in communication engineering, the advantage being that a more in-depth and accurate model can be provided. This is because the electromagnetism-based model exactly measures the electromagnetic behavior of a signal and hence, more details of the ambient environment are involved in the modeling procedure. However, it should not be tendentiously ignored that the disadvantage is also obvious. Because superabundant details should be involved, this model is sometimes inefficient and even impractical. To investigate this innovative modeling technique in more detail, we provide a simplified propagation scenario through only considering direct and single reflected paths between the transmitter and the receiver. By means of this special case study, the pros and cons of electromagnetism-based modeling can be revealed extensively. A series of familiar concepts and jargons frequently referred to in wireless mobile communication are also interpreted in view of the electromagnetism-based modeling technique. More importantly, in this paper, the nature of signal transmission and reception in free space can be analyzed in depth by virtue of this modeling technique.

Keywords: Mobile communication system · Modeling · Electromagnetic theory · Signal propagation

1 Introduction

The modeling of mobile communication systems is a frequent topic of study since the last century [1,2]. However, it is from the perspective of signals and

W. Niu et al. (Eds.): ATIS 2015, CCIS 557, pp. 280–290, 2015.
DOI: 10.1007/978-3-662-48683-2_25

systems that these conventional modeling techniques of mobile communication systems are normally derived from [3]. As a result, these conventional modeling techniques selectively ignore the details of signal propagation and the ambient environment, especially when the networking topology becomes complex [4–7]. This ambiguity is always efficient in practice, since the electromagnetic nature of signals are too complicated to study and involves Maxwell's equations [8]. Also, it is rather difficult, when modeling, to measure the ambient environment precisely and take all potential ambient factors into consideration [9]. Admittedly, it is wise to employ conventional modeling techniques when the details can be ignored and when we only need to focus on the signal input/output relation. However, resorting to these modeling techniques *de facto* degrade modeling precision and shadow the nature of a realistic mobile communication system. Moreover, when the propagation process is required to be analyzed in near field and the velocity of a mobile system is discussed in the order of speed of light levels, these traditional modeling techniques are all stranded and useless [10]. For these special cases, we should view mobile communication systems in terms of electromagnetic theory and build a series of analytical methodologies, especially in certain oversimplified cases where the electromagnetism-based modeling technique can be precise without loss of efficiency. In order to delve into the details of an electromagnetism-based modeling technique of mobile communication systems, we present a case study in this paper which only takes into consideration the direct and single reflected paths between the transmitter and the receiver. By means of this case study, the pros and cons of electromagnetism-based modeling can be revealed and a number of familiar concepts can be reinterpreted through electromagnetic theory. In addition, the nature of signal transmission and reception in free space can be analyzed in depth.

The rest of this paper is organized as follows. In Sect. 2, we present first the fundamentals of signal radiation and propagation which serve as a foundation for further modeling and analysis. Then, the detailed modeling procedure and analysis are provided in Sect. 3. Based on these constructed models, a number of relevant simulations are contacted subsequently and the simulation results are illustrated and discussed in Sect. 4. Finally we conclude this paper in Sect. 5.

2 Fundamentals of Signal Radiation and Propagation

Consider the nature of a wireless radio signal, it is essentially a high-frequency electromagnetic wave and the information contained in the signal is carried by the transmitted electromagnetic field. Three characteristic parameters, i.e. amplitude A, frequency f and phase angle Θ, specialize the carried information. Without loss of generality, we might choose a cosine waveform to express the transmitted electromagnetic field and devise its generic form by [11]:

$$E(t) = A\cos(2\pi ft + \Theta) \tag{1}$$

Assume such an electromagnetic field is transmitted from an isotropic antenna with power P_t as shown in Fig. 1, in which the transmit antenna and the

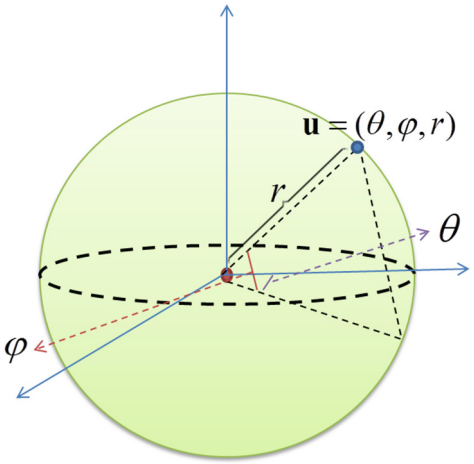

Fig. 1. Free space signal radiation model.

measured point are marked as red and blue points respectively. In the polar coordinate system, each point in free space can be characterized by a vector $\mathbf{u} = (\theta, \varphi, r)$. Assume further that the isotropic antenna is located in the origin and an arbitrary measured point is denoted by $\mathbf{u} = (\theta, \varphi, r)$. Because of the implementation of an isotropic antenna, a set of points over a spherical surface with radius r are mutually equivalent in terms of the field strength. Therefore in this case, the field strength and the received power only depend on the separation distance r between the measured point and the transmitter isotropic antenna. That is, the far field strength is uniformly distributed in free space. Consequently, the three-dimensional space of signal propagation can be reduced to a two-dimensional space. As a result, when the separation distance r is larger than the Fraunhofer distance, the far field power flux density at the measured point can be determined by [12]:

$$\Phi(r) = \frac{P_t}{4\pi r^2} \tag{2}$$

It can be proved that the captured effective area of an isotropic received antenna is [12]:

$$A_{iso} = \frac{\lambda^2}{4\pi} = \frac{1}{4\pi}\left(\frac{c}{f}\right)^2 \tag{3}$$

where λ is the wavelength of the received electromagnetic wave, i.e. the signal; c is the speed of light.

Therefore, if an isotropic antenna is employed at the measured point to receive the electromagnetic wave, the received power is:

$$P_r(r) = \Phi(r)A_{iso} = P_t\left(\frac{c}{4\pi f r}\right)^2 \tag{4}$$

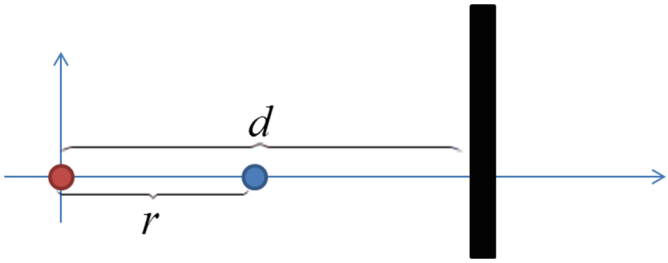

Fig. 2. Direct path and single reflected propagation model. (Color figure online)

From (4), it is clear that the power of the electromagnetic wave decreases as r^{-2}. According to (1) and the relation between the wave amplitude and the power, it is obvious that the wave amplitude decreases as r^{-1}. Therefore, we can determine the received electromagnetic field from the direct propagation path by:

$$\begin{aligned} E_{dr}(t) &= A(r)\cos[2\pi f(t - r/c) + \Theta] \\ &= \frac{A_0 \cos[2\pi f(t - r/c) + \Theta]}{r} \end{aligned} \tag{5}$$

where A_0 is termed critical amplitude, which is the amplitude at the Fraunhofer distance r_0; r_0 is the demarcation between near field and far field regions and normally we have $r_0 \gg \lambda$ [13]. In particular, we should note that the phase shift term $-2\pi fr/c$ presented in this expression is caused by the propagation delay of the electromagnetic field.

3 Modeling Procedure and Analysis

Having constructed the fundamental models of the signal radiation and propagation at the far field region of free space, let us now look into a more complicated scenario. Assume an infinitely long, hard and non-transparent plane exists as shown in Fig. 2 and that the distance between the transmit isotropic antenna and the plane is d ($d > r$). From the model constructed in Sect. 2, it is easy to derive the reflected wave detected at the measured point:

$$E_{rr}(t) = -\frac{A_0 \cos[2\pi f(t - (2d - r)/c) + \Theta]}{2d - r} \tag{6}$$

According to the linearity of the electromagnetic field at the far field region, the superposition of the field strengths from the direct propagation path and the reflected path can be calculated by:

$$\begin{aligned} E_r(t) &= E_{dr}(t) + E_{rr}(t) \\ &= \frac{A_0 \cos[2\pi f(t - r/c) + \Theta]}{r} \\ &- \frac{A_0 \cos[2\pi f(t - (2d - r)/c) + \Theta]}{2d - r} \end{aligned} \tag{7}$$

Furthermore, if we assume that the measured point is moving towards the plane at a constant speed v, the propagation process becomes time-varying and the time-varying separation distance can be expressed by $r = r_1 + vt$, where r_1 is the initial separation distance and satisfies the condition $r_1 > r_0$. As a consequence, (7) can be rewritten as:

$$\begin{aligned} E_r(t) = &\frac{A_0 \cos[2\pi f(t - (r_1 + vt)/c) + \Theta]}{r_1 + vt} \\ &- \frac{A_0 \cos[2\pi f(t - (2d - r_1 - vt)/c) + \Theta]}{2d - r_1 - vt} \end{aligned} \tag{8}$$

From (8), because c is a constant as a basic axiom of the special theory of relativity (STR), it thereby cannot be varied by human factors [14]. Therefore, the received resultant field strength of this two-path scenario is determined by r_1, A_0, f, v, t and Θ. More generally and precisely, we might replace $E_r(t)$ by $E_r(r_1, A_0, f, v, t, \Theta)$. However, since A_0 is mainly determined by the transmitter power and only serves as a linear scaler of $E_r(r_1, A_0, f, v, t, \Theta)$, for brevity, we might suppose it to 1 (normalized). Also, because the phase angle is relative and quite arbitrary, without loss of generality, we may specify it as 0. Analogously, r_1 can also be viewed as a constant for the purpose of simplification.

These three clarified conditions result in an elucidation of the analysis and now the received resultant field strength is only associated with f, v and t. Consequently, the general form of the received resultant field strength $E_r(f, v, t)$ can be expressed by:

$$\begin{aligned} E_r(f, v, t) = &\frac{\cos[2\pi f(t - (r_1 + vt)/c)]}{r_1 + vt} \\ &- \frac{\cos[2\pi f(t - (2d - r_1 - vt)/c)]}{2d - r_1 - vt} \end{aligned} \tag{9}$$

By variable control, it is easy to investigate into the effects of these three variables on the received resultant field strength $E_r(f, v, t)$.

4 Simulation and Discussion

To simulate the time-varying property of the mobile communication system constructed above, we first set $f = 9.6$ GHz and $v = 1$ m/s. Further assume the diameter of the transmit isotropic antenna $D = 0.5$ m. Therefore, in this case, the Fraunhofer distance can be determined by [15]:

$$r_0 = \frac{2D^2}{\lambda} = \frac{2D^2 f}{c} = 16 \text{ m} \tag{10}$$

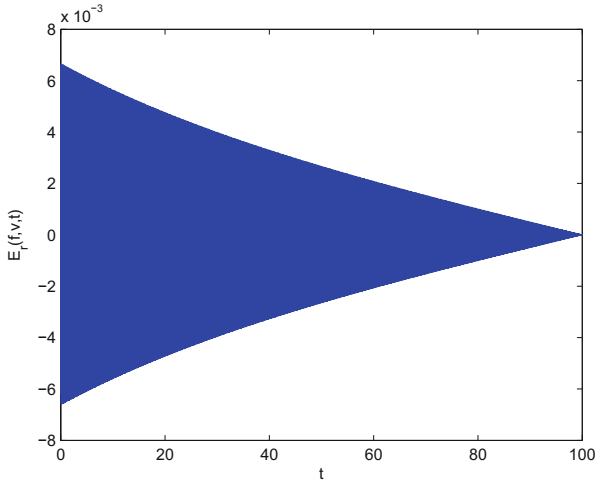

Fig. 3. Simulation of large-scale time variation, providing $f = 9.6$ GHz, $v = 1$ m/s, $r_1 = 100$ m and $d = 200$ m.

From (10), it is reasonable to set $r_1 = 100$ m and $d = 200$ m. Having done so, we can simulate the relation between the received resultant field strength $E_r(f, v, t)$ and the only variable t. The large-scale time variation results are plotted in Fig. 3. From this figure, it is clear that as the moving measured point approaches the reflection plane, these two electromagnetic waves completely cancel each other out and the received resultant field strength $E_r(f, v, t)$ equalts to $o[E_r(f, v, 0)]$. However, one might argue that the decay of the field strength is caused by the enlarged separation distance $r = r_1 + vt$ over time. This argument is correct to some extent, but it should be noted that only the counteraction of two identical electromagnetic waves caused by ideal reflection can yield $E_r(f, v, t) = o[E_r(f, v, 0)]$. To verify this conjecture, let us remove the reflection plane and re-simulate under the same conditions. The simulation results are illustrated in Fig. 4. From this figure, our conjecture has been validated, and the attenuation as r^{-1} is trivial in comparison with $o[E_r(f, v, 0)]$.

To investigate the time-varying property in more detail, we carry out a further small-scale time variation simulation and plot the results in Fig. 5. In this particular case, the impact of the separation attenuation r^{-1} on $E_r(f, v, t)$ is supposed to be negligible. In fact, the high-frequency vibration of $E_r(f, v, t)$ is caused by the displacement of the measured point over time. Once $t = \arg\left\{\frac{\cos[2\pi f(t-(r_1+vt)/c)]}{r_1+vt} = \frac{\cos[2\pi f(t-(2d-r_1-vt)/c)]}{2d-r_1-vt}\right\}$, the direct and reflected electromagnetic waves will add destructively and cancel each other out. At this instant in time, the received field strength equals to $o[E_r(f, v, 0)]$ and the received signal is too weak to be precisely detected. Intuitively, the communication reliability will be significantly hindered. On the other hand, the direct wave and the reflected wave can also add constructively causing the received field strength to

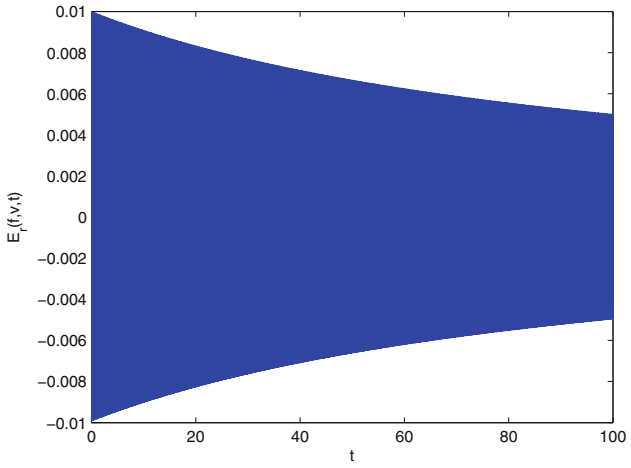

Fig. 4. Simulation of large-scale time variation, providing $f = 9.6$ GHz, $v = 1$ m/s, $r_1 = 100$ m and $d = \infty$.

reach a peak for which the received signal can then be detected with more ease. This vibration phenomenon of $E_r(f, v, t)$ reflects the nature of multipath fading and the distance from a valley to a peak is defined as the coherence distance [3]:

$$\Delta r_c = \frac{\lambda}{4} = \frac{c}{4f} \tag{11}$$

From (11), normally Δr_c is relatively small compared to the antenna coverage [3]. Hence, multipath fading is also termed small-scale fading, since the amplitude of the received signal varies tempestuously within several meters. On the contrary, the envelope attenuation as r^{-1} illustrated in Fig. 4 is termed large scale fading, since it will only become significant when the displacement of the measured point is notably larger then the coherence distance Δr_c. Similarly, we can also understand the nomenclature and classification of slow and fast fading.

Akin to the variable control strategy as we have used above, we now fix t to 0 and vary carrier frequency f within the region $[8.5, 9.6]$ GHz, The simulation results are presented in Fig. 6. As shown in this figure, the drastic fluctuation shuttling $o[E_r(f, v, t)]$ back and forth is expected, since the compensation mechanism of two waves can still be activated by the variation of carrier frequency even though the measured point remains motionless. Similarly, the frequency difference between the valley and the peak of $E_r(f, v, t)$ is fixed and termed coherence bandwidth [3]:

$$\Delta f_c = \frac{1}{2}\left(\frac{2d - r_1}{c} - \frac{r_1}{c}\right)^2 \tag{12}$$

Finally, we set f back to 9.6 GHz again and allow the speed of the measured point v to vary within [0, 100]. Furthermore, in order to prevent the collision

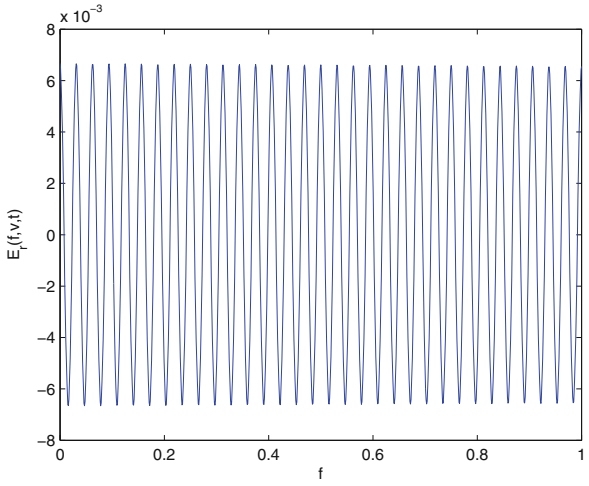

Fig. 5. Simulation of small-scale time variation, providing $f = 9.6$ GHz, $v = 1$ m/s, $r_1 = 100$ m and $d = 200$ m.

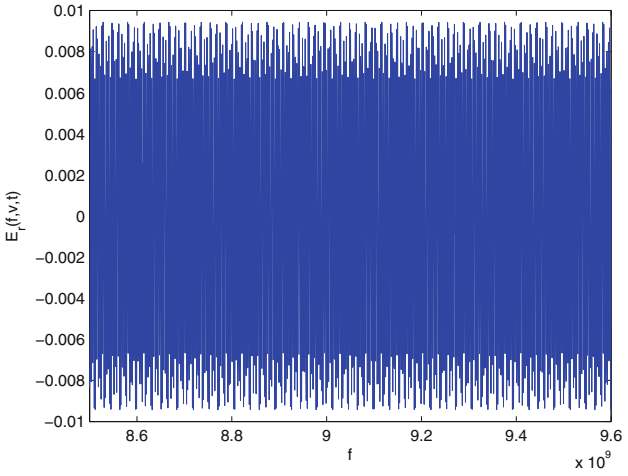

Fig. 6. Simulation of frequency variation, providing $t = 0$, $v = 1$ m/s, $r_1 = 100$ m and $d = 200$ m.

between the measured point and the reflection plane, we reset $d = 2000$. The simulation in this case is conducted and the results are illustrated by a 3D plot and a contour in Figs. 7 and 8 respectively. From these figures, several important points can be summarized. Firstly, the effects of speed v and time t are symmetrical and this can be interpreted by the equivalent coherence distance mechanism activated by the variations of v and t. In addition, the impact of the variation of v has a negligible influence on the small-scale fading but an evident

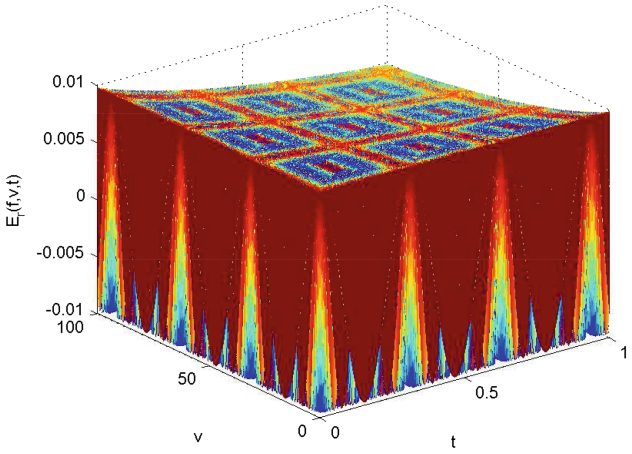

Fig. 7. Simulation 3D plot of the relation among v, t and $E_r(f, v, t)$, providing $f = 9.6$ GHz.

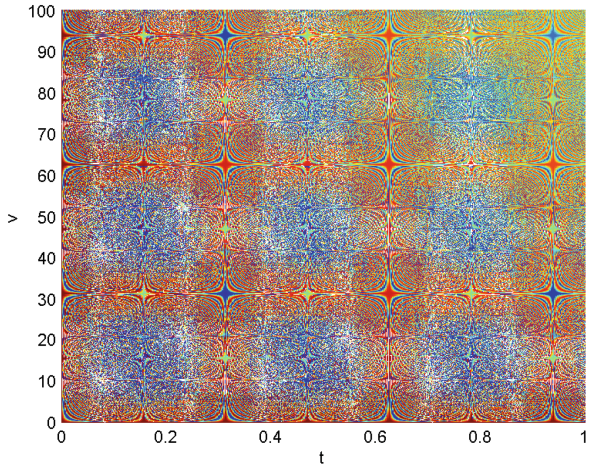

Fig. 8. Simulation contour plot of the relation among v, t and $E_r(f, v, t)$, providing $f = 9.6$ GHz.

impact on the large-scale fading. This is because the small-scale fading mainly depends on the frequency property of the resultant electromagnetic wave, while the Doppler shift (frequency deviation caused by the movement) at the low speed condition ($v \ll c$) is trivial compared to the carrier frequency f adopted in this example. The impact of the Doppler shift caused by movement at the speed v can be qualified by Doppler spread [3]:

$$D_s(f, v) = |\Delta f_{dd}(f, v) - \Delta f_{rd}(f, v)| = \frac{2fv}{c} \tag{13}$$

where $\Delta f_{dd}(f, v)$ is the Doppler shift of the direct wave and $\Delta f_{rd}(f, v)$ is the Doppler shift of the reflected wave.

In this simulation example, $D_s(f, v) \in [0, 6400]$ Hz $\ll f = 9 \times 10^9$ Hz. This result quantitatively explains the reason why Doppler shift can always be ignored in practice when analyzing small-scale fading [12].

5 Conclusion

In conclusion, we have constructed a simplified model of mobile communication systems through the application of electromagnetic theory. Although we have illustrated this model in an oversimplified case where only two-path electromagnetic waves are considered, this paper can still serve as a firm reference for more complicated scenarios. Furthermore, compared to conventional signal system models, the electromagnetic nature of signals and a series of phenomena can be explained and analyzed more extensively by this electromagnetism-based model. However, we can also notice that even for this oversimplified scenario, the electromagnetism-based model is complicated and thus might not be applicable when the ambient environment is complex.

References

1. Proakis, J., Salehi, M.: Digital Communications. McGraw-Hill Education, New York (2007)
2. Lv, Z., Feng, L., Feng, S., Li, H.: Extending touch-less interaction on vision based wearable device. In: IEEE Virtual Reality Conference, France (2015)
3. Tse, D., Viswanath, P.: Fundamentals of Wireless Communication. Cambridge University Press, New York (2005)
4. Ma, Z.X., Zhang, M., Shaham, S., Dang, S.P., Hart, J.: Literature review of the communication technology and signal processing methodology based on the smart grid. Appl. Mech. Mater. **719**, 436–442 (2015)
5. Guo, P., Bai, Y., Ma, Z., Wu, S., Dang, S.: Relay technology for multi-carrier systems: A research overview. In: 2015 Third International Conference on Computer, Communication, Control and Information Technology (C3IT), pp. 1–5. IEEE (2015)
6. Dang, S., Coon, J.P., Simmons, D.: Combined bulk and Per-Tone relay selection in super dense wireless networks. In: IEEE ICC 2015, London, United Kingdom (2015)
7. Ma, Z., Gholamzadeh, A., Tang, B., Dang, S., Yang, S.: Matlab based simulation of the efficiency of the complex OFDM on power line communication technology. In: 2014 Fourth International Conference on Instrumentation and Measurement, Computer, Communication and Control (IMCCC), pp. 374–378. IEEE (2014)
8. Johler, J.: Propagation of the low-frequency radio signal. Proc. IRE **50**, 404–427 (1962)
9. Hashemi, H.: The indoor radio propagation channel. Proc. IEEE **81**, 943–968 (1993)
10. Sobot, R.: Wireless Communication Electronics: Introduction to RF Circuits and Design Techniques. Springer, New York (2012)

11. Clemmow, P.: An Introduction to Electromagnetic Theory. Cambridge University Press, Cambridge (1973)
12. Rappaport, T.: Wireless Communications: Principles and Practice, 2nd edn. Prentice Hall PTR, Upper Saddle River (2001)
13. Balanis, C.: Antenna Theory: Analysis and Design. Wiley, New York (2012)
14. Banerjee, B., Banerjee, A.: The Special Theory of Relativity. Prentice Hall India Pvt., Limited, Upper Saddle River (2004)
15. Cheng, D.: On the simulation of Fraunhofer radiation patterns in the Fresnel region. IRE Trans. Antennas Propag. **5**, 399–402 (1957)